Resonant random phase approximation

P. Curutchet, T. Vertse,* and R. J. Liotta

Research Institute of Physics, S-10405 Stockholm, Sweden

(Received 3 October 1988)

Particle-hole excitations are studied in terms of a single-particle representation consisting of bound states and resonant solutions (Gamow resonances) of a "realistic" Woods-Saxon potential. Within this representation a particle-hole resonant random phase approximation is developed. Using the resonant random phase approximation the escape widths of the multipole giant resonances in ^{208}Pb are calculated and reasonable agreement with available experimental data is obtained.

I. INTRODUCTION

Many observed nuclear properties have features which cannot be described without a proper inclusion of excitations in the continuum. Although methods like continuum shell model,[1] continuum random phase approximation (RPA),[2-4] coupled channels,[5] and time-dependent Hartree-Fock calculations[6] have proved to be successful in treating the continuum, they involved rather cumbersome and extremely time-consuming calculations. Besides, many details of the underlying microscopic structure remain hidden within these approaches due to a treatment of the continuum which is not able to differentiate background from resonant features.[7] Only recently did calculations done within the continuum RPA seem to disentangle these two processes.[8]

One so far open question strongly connected with this problem concerns the particle decay of giant resonances (GR's). GR's show up as broad bumps in the nuclear spectra above the neutron emission threshold and their width is composed of two important parts: the "escape width" $\Gamma^\uparrow$, which represents the coupling to the continuum, and the spreading width $\Gamma^\downarrow$ measuring the coupling to two-particle–two-hole and more complex configurations. The GR's can decay by particle emission or by γ radiation. Though their electromagnetic decay has been thoroughly studied, it was only recently that new experimental setups allowed us to investigate particle emission in the decay of giant monopole and quadrupole resonances.[9-13] One is thus confronted with the task of developing microscopic theories which would provide a suitable description of the particle emission decay of the GR's. Our aim in undertaking this task has been to account for the most apparent effects of the continuum in an economical and feasible manner which at the same time yields some insight into how GR's are built out of particle-hole excitations. In order to achieve these goals, proposed in Ref. 14 was a fast approximate method that we called *resonant* RPA (RRPA). In that reference the accuracy of the RRPA was tested by comparing its result to that of "exact" methods [the continuum RPA (Ref. 3) and coupled channels calculations[5]] for the dipole GR in ^{16}O. A brief summary of the method was also given there and the power of the RRPA was shown for heavy nuclei (the isoscalar quadrupole GR in ^{208}Pb).

In the RRPA the single-particle basis is composed of bound single-particle states and single-particle resonant (Gamow) states. We will denote this set of states by GS. With the GS the completeness relation of Berggren[15] is used together with regularization methods for calculating the divergent integrals. The use of Gamow states automatically takes care of the possibility of particle emission from the unbound particle states. An advantage of the RRPA method is that after neglecting the effect of a complex continuum we deal only with discrete eigenstates of the single-particle Hamiltonian; therefore methods well known from nuclear structure calculations can still be used. The price we pay for this convenience is that our method is an approximate one. The continuum itself has a structure since it contains a background and several single-particle resonances. Through the resonant basis states the RRPA includes the effect of the narrow resonances in the region of the giant resonance but not the effect of the slowly varying background. In this way the RRPA is able to describe a major part of the escape width and the fragmentation of the multipole strength (Landau damping), and at the same time it opens certain insight into the building up and the decay of the GR's.

The use of GS's as a single-particle representation is a novel and important ingredient in this paper. Yet, Gamow resonances were introduced in nuclear physics long ago in connection with spontaneous alpha decay.[16] However, their use was hindered by the lack of a regularization procedure to calculate their norm. Even after this problem was solved there was some reluctance to use GS's to describe spectroscopic properties connected with the continuum. The main reason for this was that GS's are orthogonal to any real continuum state.[15] But recently it was shown that Gamow resonances have the peculiar property that although they are orthogonal to any real state, they are not orthogonal to wave packets formed from a superposition of continuum states.[17] Another peculiar property which is important for our purposes is that Gamow resonances have a large overlap with wave packets that are peaked at the resonance energy.[17] Therefore, the inclusion of GS's would be equivalent to the use of bound states and of a set of wave packets centered in the *resonant* energies corresponding to the realistic potential used to obtain the GS's. In other words, it makes sense to describe observable states using wave

packets connected with the same main field which induces those states.

In Sec. II of this paper we review the definition and basic properties of Gamow functions, the generalization of the scalar product that should be applied when handling them, and the completeness relation of Berggren.[15] In Sec. III we show how the use of these complex states modifies the standard RPA equations and discuss the solution of the RRPA equations. We apply the RRPA method in Sec. IV for the calculation of GR's of different multipolarities in ^{208}Pb. In the last section a summary of the results and the conclusions are given.

II. GAMOW RESONANCES:
REVIEW OF BASIC CONCEPTS

This section will be devoted to summarizing the basic definitions and establishing the notations which we will adopt when referring to our single-particle representation.

For simplicity we consider as our system a spinless particle moving in a spherically symmetric potential $V(r)$ which is the sum of a short-range nuclear and an infinite range Coulomb term, i.e., $V(r) = V_N(r) + V_C(r)$, which satisfies $V_N(r) = 0$ if $r > a$ and $V_C(r) = Z_1 Z_2 e^2 / r$ for $r \geq a$. The solution of the Schrödinger equation $H\Psi = E\Psi$ can be expanded in partial waves u_l that will be solutions of the radial equation

$$u_l''(r,k) + \left[k^2 - \frac{l(l+1)}{r^2} - U(r) \right] u_l(r,k) = 0 , \quad (1)$$

where $c = 2\mu/\hbar^2$, $U(r) = cV(r)$, $k^2 = cE$, and μ is the reduced mass.

The solution must be regular at the origin,

$$u_l(0,k) = 0 , \quad (2)$$

and for $r \geq a$ it can be expressed by the two linearly independent Jost solutions or the O_l and I_l outgoing and incoming Coulomb waves and the S matrix as follows:

$$u_l(r,k) = x_l(k) O_l(kr) + y_l(k) I_l(kr) , \quad (3)$$

$$u_l(r,k) = y_l(k) [I_k(kr) - S_l(k) O_l(kr)] , \quad (4)$$

where $S_l = -x_l / y_l$ and for large distances $O_l \rightarrow e^{i\theta}$, $I_l \rightarrow e^{-i\theta}$ with

$$\theta = kr - \eta \ln 2kr - l\pi/2 + \sigma_l .$$

All the parameters appearing in the definition of θ are the usual ones in scattering theory: η is Sommerfeld parameter and σ_l the Coulomb phase shift.

Imposing the Siegert boundary condition[18] of having only outgoing waves at infinity [i.e., $y_l(k) = 0$], which is satisfied for only those points k_n of the complex k plane where S_l has a pole, three types of solutions are obtained corresponding to bound states $(k_n = i\gamma_n)$, antibound states $(k_n = -i\gamma_n)$, and resonances $(k_n = \pm\kappa_n - i\gamma_n)$. In all cases γ_n is greater than 0. Since the asymptotical behavior is governed by $O_l(kr) \rightarrow e^{ikr}$, it is clear that only the bound states are square integrable since they behave

as $e^{-\gamma_n r}$, while the antibound states behave like $e^{\gamma_n r}$. The Gamow resonances which are lying on the lower half of the k plane in pairs, $k_n = \kappa_n - i\gamma_n$ and $\tilde{k}_n = -\kappa_n - i\gamma_n = -k_n^*$, also diverge for increasing values of r as $u_l(r,k_n) \rightarrow e^{\gamma_n r} e^{i\kappa_n r}$ and $\tilde{u}_l(r,\tilde{k}_n) \rightarrow e^{\gamma_n r} e^{-i\kappa_n r}$.

The function u_l with $\text{Im}(k_n^2) < 0$ represents a decaying state because the time dependence of the solution with the complex energy

$$E_n = \frac{1}{c} k_n^2 = \epsilon_n - i\Gamma_n/2$$

becomes

$$e^{-iE_n t/\hbar + ik_n r} = e^{-\Gamma_n t/2\hbar} e^{\gamma_n r} e^{i(\kappa_n r - \epsilon_n t/\hbar)} . \quad (5)$$

The decay in the wave function is exponential with a relaxation time $\tau = 2\hbar/\Gamma_n$. The increase of the amplitude with r is due to the fact that the outgoing particle has a finite velocity so that a particle which is observed now at a position r left the origin a time Δt before, when the source was stronger by a factor of $e^{\Gamma_n \Delta t/2\hbar} = e^{\gamma_n r}$, as first realized by Gamow.[6]

The time behavior of the *mirror* state $\tilde{u}_l(r,\tilde{k}_n) = u_{l,k_n}^*(r)$, $\tilde{k}_n = -k_n^*$,

$$\tilde{E}_n = \frac{1}{c} \tilde{k}_n^2 = \epsilon_n + i\Gamma_n/2$$

is just the opposite

$$e^{-i\tilde{E}_n t/\hbar + i\tilde{k}_n r} = e^{\Gamma_n t/2\hbar} e^{\gamma_n r} e^{-i(\kappa_n r + \epsilon_n t/\hbar)} \quad (6)$$

and therefore it represents a "capturing state" growing exponentially in time.

Since the complex energy eigenvalues can have only discrete values, resonance states resemble bound states rather than scattering states having continuous spectra. Resonances can be considered as generalizations of the bound states since they satisfy the same equation and the same boundary conditions as the bound states, namely they are regular at $r = 0$ and behave as outgoing spherical waves beyond the range of the nuclear potential. For $\Gamma_n \ll \epsilon_n$ Gamow functions are very similar to bound state wave functions inside the nuclear potential apart from a small imaginary component. However, at large distances they oscillate with exponentially growing amplitude, as we can see in Eqs. (5) and (6), and therefore they are not square integrable.

With the traditional definition of scalar or inner product

$$\langle u_2 | u_1 \rangle = \int_0^\infty u_2^*(r) u_1(r) dr , \quad (7)$$

only the bound states can be normalized in an infinite interval. Therefore the definition of the scalar product should be generalized. The generalization of the scalar product can only be done if we use a *biorthogonal* basis and apply some *regularization* method for calculating the resulting integrals, which often diverge without regularization. Several prescriptions have been proposed for regularization (e.g., the use of convergence factors,[15,19] analytical continuation,[20] complex rotation techniques,[21] etc.). These methods differ from each other in the

mathematical techniques used and in how suitable they are when the numerical calculation of a given integral arises. They have different ranges of applicability, but practically all of them lead to the same result when they can be applied. In this work we use the method of complex rotation suggested in Ref. 21 which became later known as *exterior complex scaling*.[22] It is extremely powerful for the potentials used in nuclear physics where nuclear interactions die out beyond a finite distance a and only the long-range Coulomb potential survives. The regularization method rotates the radial distance r with a suitable angle φ only beyond this distance a, i.e., it uses the transformation

$$r \rightarrow \begin{cases} r \text{ for } r \leq a \\ a + |r - a|\exp(i\varphi) \text{ for } r > a , \end{cases} \tag{8}$$

where $\varphi < \pi/2$. Due to the dilation analyticity of the Coulomb potential $V_C(r) = Z_1 Z_2 e^2/r$, this transformation is equivalent to the exterior complex scaling of the Hamiltonian valid in the asymptotic region. In this way the results do not depend on the analytical properties of the short-range part of the potential and we can use the fact that the resonant poles k_n uncovered by the complex rotation will not change their position, as it should be according to the Aguilar, Balslev, and Combes (ABC) theorem.[23] The transformed radial wave functions will be square integrable if $\varphi > -\arg(k_n)$. Since the complex rotation gives the same result for the norm as the use of a convergence factor of the form[21] $e^{-\epsilon r^p}$, we can use the completeness relation of Berggren.[15] He formed a biorthogonal set from bound states and two types of resonances (decaying and capturing ones) by using a regularization method[19] with a Gaussian convergence factor. The resonances included in his set were selected by defining a curve $L = L^+ + L^-$ of the complex k plane like the one shown in Fig. 1. The L contour is symmetric with respect to the origin, i.e., if $k \in L^+$ then $-k \in L^-$ and its slope is limited by the condition $\arg(k) > -\pi/4$. The completeness relation of Berggren states that

$$\delta(r - r') = \sum_n \tilde{u}_n^*(r, \tilde{k}_n) u_n(r', k_n)$$
$$+ \int_{L^+} \tilde{u}^*(r, k) u(r', k) dk \tag{9}$$

acts as a unit operator in the space of all states whose radial component goes asymptotically to zero faster than any exponential or behaves as e^{ikr} with k values lying above the contour L. The summation in Eq. (9) refers to all bound states and the selected set of decaying resonances with k_n between L^+ and the real axis. The introduction of the contour L suits our purpose of neglecting the integral of the scattering states $u(r,k)$ in Eq. (9) and using only the finite sum of the first term. We have a great flexibility in choosing the contour L, i.e., in deciding which are the resonances we include into the basis. We have to select those resonances which are relevant for the physical problem under consideration. The inclusion of Gamow resonances to some extent is equivalent to the use of a set of wave packets centered in the *resonant* ener-
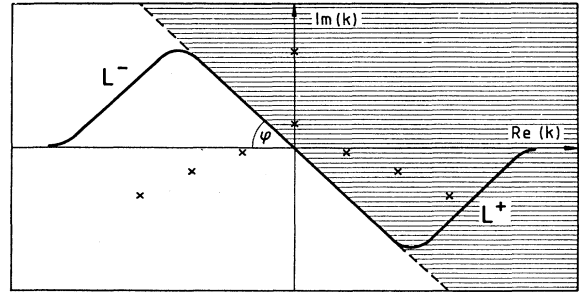
FIG. 1. Integration contour L for the completeness relation of Eq. (9). Crosses denote the poles of the scattering function $S_l(k)$. Pole solutions falling into the shadowed area are square integrable if we apply the complex rotation of Eq. (8).

gies. Romo showed[17] that though a Gamow resonance is orthogonal to any real continuum state, it has a large overlap with a wave packet which is formed from a superposition of continuum states and is peaked at the resonant energy.

III. RESONANT RPA

A. Formalism

Since in Sec. II we introduced a generalized scalar product which differs from the standard one, we will give here some details of the particle-hole RRPA formalism that will be applied in the next section.

As in the calculation of bound states, we define within our GS representation the Fermi level and the hole and the particle states according to the number of particles that our system contains. We then linearize the particle-hole equation of motion to obtain the RPA equations. The corresponding particle-hole (forward) amplitudes X_n and hole-particle (backward) amplitudes Y_n are obtained from the RRPA equations

$$\begin{bmatrix} A & B \\ -B & -A \end{bmatrix} \begin{bmatrix} X_n \\ Y_n \end{bmatrix} = W_n \begin{bmatrix} X_n \\ Y_n \end{bmatrix} , \tag{10}$$

which has a form which is similar to the standard RPA equations.[24] The difference is that no complex conjugation operation appears in Eq. (10) and the matrix elements of the matrices A and B should now be calculated using the complex rotation technique according to the definition of the generalized scalar product as we have discussed before. This also applies to the RPA normalization condition that now is

$$X_n^T X_n - Y_n^T Y_n = 1 \tag{11}$$

and *not* $X_n^{T*} X_n - Y_n^{T*} Y_n = 1$, as it would be in a standard representation. In the biorthogonal basis the spin and angular parts of the matrices A and B are the same as in the bound single-particle representation, and the difference only appears in the radial integrals, which now read

$$I_{pqrs} = \text{reg} \int_0^\infty r_1^2 dr_1 \int_0^\infty r_2^2 dr_2 R_p(r_1)R_q(r_2)$$
$$\times V(r_1,r_2)R_r(r_1)R_s(r_2) , \qquad (12)$$

where reg means that the regularization procedure is applied if needed. The angle φ of the complex rotation is chosen so that all kinds of radial wave functions (bound states and resonances) go to zero along the complex path of Eq. (8), i.e.,

$$\varphi = \tfrac{1}{2}\max|\arg(k_n)| + \frac{\pi}{4} . \qquad (13)$$

The radial part of the single-particle wave function is, as usual,

$$R_i(r) = \frac{u_i(r,k_i)}{r} . \qquad (14)$$

Using the condition (13) the calculation of the interaction matrix elements (12) can be performed without major difficulties. Explicit expressions for the particle-hole Migdal interaction were given in Ref. 25. In the applications below we use the multipole-multipole interaction, i.e.,

$$V_\lambda = -\kappa_\lambda Q_\lambda Q_\lambda , \qquad (15)$$

where κ_λ is the strength of the force and Q_λ is the multipole operator

$$Q_{\lambda\mu} = f_\lambda(r)Y_{\lambda\mu}(\hat{r}) . \qquad (16)$$

For the radial dependence we use

$$f_\lambda(r) = r\frac{\partial V(r)}{\partial r} , \qquad (17)$$

where

$$V(r) = \frac{V_0}{1 + e^{(r-R)/a}} \qquad (18)$$

or

$$f_\lambda(r) = r^\lambda . \qquad (19)$$

Within the separable interaction (15) the radial integral can be written as

$$I_{pqrs} = M_{pr}M_{qs} , \qquad (20)$$

where

$$M_{pr} = \text{reg} \int_0^\infty r^2 dr \, R_p(r)f_\lambda(r)R_r(r) , \qquad (21)$$

and the RPA eigenvalue problem (10) reduces to the well-known dispersion relation[26,27]

$$F_\lambda(W) = \sum_{ki} \frac{2(\epsilon_k - \epsilon_i)\langle k|Q_\lambda|i\rangle^2}{W^2 - (\epsilon_k - \epsilon_i)^2} , \qquad (22a)$$

$$F_\lambda(W_n) = \frac{1}{\kappa_\lambda} ; \qquad (22b)$$

where W_n is the complex energy of the state n. It is clear that $\text{Re}(W_n)$ is the position of the resonance and $\text{Im}(W_n)$ is half of its escape width. The solution of the complex dispersion relation will be discussed in detail in the next

section.

Since Q_λ is also the transition operator of relevance in the decay of particle-hole states, the energy-weighted sum rule[28]

$$S(Q) = \tfrac{1}{2}\langle 0|[Q,[H,Q]]|0\rangle = \sum_n W_n\langle n|Q|0\rangle^2 \qquad (23)$$

can be calculated by using Eq. (21). In the applications below we have checked that this sum rule is independent of the isospin character of the operator as well as of any local interaction.[24]

While the real part of the strength function measures the concentration of the multipole strength on the state concerned, it is not completely clear what interpretation should be assigned to the imaginary part of the strength function and, in general, to the imaginary part of any transition probability. A reasonable interpretation of this quantity is that it is related to the uncertainty of the interference between the resonance and the background of the process being studied.[29] Within this interpretation, the larger the imaginary part of the quantity, the larger the uncertainty of the value given by the real part.

B. Complex dispersion relation

In the standard case of real representations the solution of Eq. (22) can be conveniently performed graphically as the intersection of the curve $F_\lambda(W)$ with the horizontal line $1/\kappa_\lambda$. In our case, however, all quantities in Eq. (22) are complex and those curves become surfaces in the complex space. The real and the imaginary parts of F_λ are surfaces with singularities at the unperturbed particle-hole energies $W = \pm(\epsilon_k - \epsilon_i)$. An example of this is shown in Fig. 2. The RRPA solutions are provided by the complex values W_n which simultaneously solve the equations

$$\text{Re}(F_\lambda(W_n)) = \text{Re}(1/\kappa_\lambda) , \qquad (24a)$$

$$\text{Im}(F_\lambda(W_n)) = \text{Im}(1/\kappa_\lambda) . \qquad (24b)$$

Due to the complicated structure of the dispersion relation we could not find all its roots in realistic cases by using root finding methods of transcendental equations. We then decided to diagonalize the RRPA matrix directly using standard complex diagonalization routines.[31] However, it is interesting to analyze how collectivity is built up in the case of a complex dispersion relation. Therefore here we will make a qualitative analysis.

The W_n values satisfying Eq. (24a) lie on the intersection of the surface $\text{Re}(F_\lambda(W))$ and the plane $\text{Re}(1/\kappa_\lambda)$. Let us call this intersection C_R. Then C_I is defined analogously by Eq. (24b). The curves C_R and C_I are shown as dotted and full lines, respectively, in Fig. 3. The roots of Eq. (24) are the points lying both on C_R and C_I: $W_n \in C_R$, $W_n \in C_I$. With weak interaction κ_λ the planes $\text{Re}(1/\kappa_\lambda)$ and $\text{Im}(1/\kappa_\lambda)$ cut the surfaces $\text{Re}(F_\lambda(W))$ and $\text{Im}(F_\lambda(W))$ at large values where, as it can be seen from Fig. 2, C_R and C_I are closed loops around the unperturbed energies. Increasing the strength, the planes corresponding to $1/\kappa_\lambda$ approach the
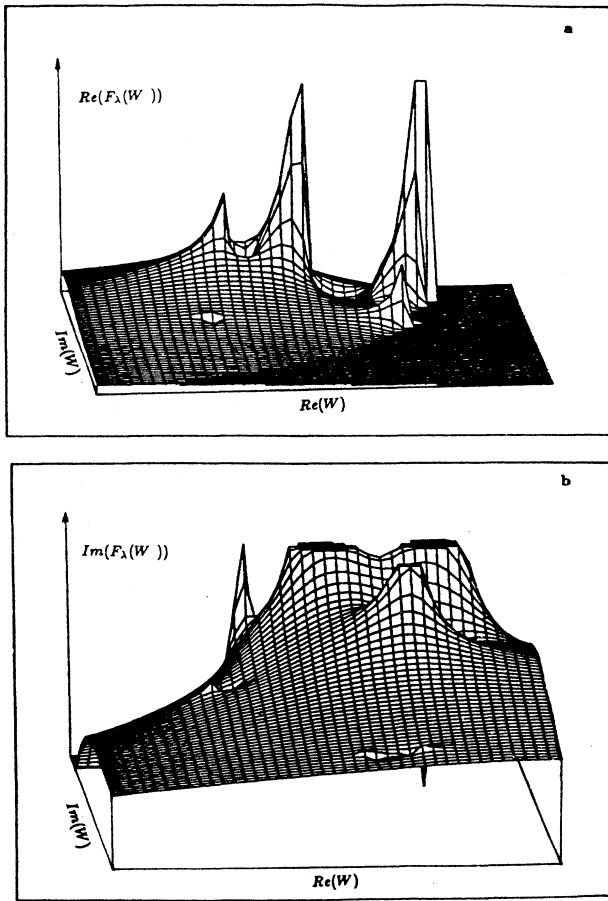
FIG. 2. Real (a) and imaginary (b) part of the function $F_\lambda(W)$, Eq. (22a). The strong peaks in this figure correspond to the singularities at the unperturbed particle-hole energies.

FIG. 3. Graphical solution of the dispersion relation Eq. (24). The intersection C_R of the surface $\mathrm{Re}(F_\lambda(W))$ with the horizontal plane $\mathrm{Re}(1/\kappa_\lambda)$, Eq. (24a), is the dashed line, while the full line is the intersection C_I corresponding to the imaginary parts $\mathrm{Im}(F_\lambda(W))$ and $\mathrm{Im}(1/\kappa_\lambda)$, Eq. (24b). The points where C_R and C_I crisscross (denoted by dots) are the W_n values, i.e., the solutions of the dispersion relation.

"ground level" where, according to Eq. (24), $F_\lambda(W)=0$. If the plane cuts hills standing alone (Fig. 2), the roots remain close to the particle-hole energy and the solutions are noncollective. On the other hand, we see in Fig. 2 that a large mountain is formed from many of the individual peaks. If we cut this mountain at its foot (that is, large values of κ), the intersection occurs far from the poles. The root corresponding to this situation has a collective feature since many particle-hole states contribute to its formation. The roots corresponding to the steep peaks are weakly dependent upon changes in the strength of the interaction because the walls of the peak are practically perpendicular to the complex plane. The root corresponding to the mountain is strongly dependent upon changes in the strength because it lies on the smooth slope of the mountain. The larger the strength, the farther the collective root is from the noncollective ones.

Within a harmonic oscillator basis, the energy of the collective state is always the lowest state within the harmonic oscillator ΔN excitation[26,27] considered (for isoscalar excitations, while for isovector excitations the collective state is the most excited one[30]). In our case, however, the collective state usually lies among noncollective

states, as seen, e.g., in Table III. This is a rather remarkable difference between the two cases.

IV. APPLICATIONS

A. Choice of the basis

We present in this section applications of the RRPA that we performed in the experimentally well-explored case of ^{208}Pb, where "exact" treatments would be difficult to carry out. We have also applied our method to light nuclei, where calculations are easier to perform. In particular, good agreement with experimental data was obtained[14] in ^{16}O.

To obtain the Gamow states we solved the one-particle Schrödinger equation using a Woods-Saxon potential with parameters shown in Table I. This calculation was done with the computer code GAMOW.[32] The calculated states are shown in Table II. One sees in this table that the bound state energies are approximately the same as in a previous calculation.[33] But from the point of view of our method, the important states are those lying in the continuum. As expected, states with high orbital angular momentum have small width due to the centrifugal barrier. The same effect is produced by the Coulomb barrier, as is also seen in Table II.

As suggested by the adequacy of the shell model to describe nuclear properties, we choose as basis states those GS which are closest to the Fermi level. In other words, we order our GS according to increasing values of the real parts of the energies (ϵ_R). States with values of ϵ_R

TABLE I. Woods-Saxon parameters for the potential used to generate the GS in ^{208}Pb. The notation and the units, i.e., MeV for energies and fm for distances, are standard.

Particle	V_0	r_0	a	V_{so}	r_c
Neutron	44.40	1.27	0.70	16.5	
Proton	66.04	1.19	0.75	19.0	1.19

differing enough from the energy of the Fermi level are assumed to be irrelevant. This criterion, which is a natural extension of the shell-model criterion, leaves the imaginary part of the single-particle energies (ϵ_I) untouched. However, there may appear GS which are so wide that they would belong rather to the proper continuum. The inclusion of these states in the single-particle representation would be against our intention of disentangling observable processes from the continuum background. Besides, we strive to use a set of GS as small as possible because we thereby expect to gain physical insight into the structure of observable states.

The adoption of a criterion to select GS with adequate values of ϵ_I is not as straightforward as it is for ϵ_R. There are several possibilities to make this selection. Observable resonances are usually narrower than the corresponding energy centroids, and only a fraction of the width corresponds to the escape width. Therefore, a reasonable criterion may be to include in the set of GS only those states that fulfill the condition $|\epsilon_I| < \epsilon_R$. But there might exist GS lying very close to the continuum threshold (i.e., with very small positive values of ϵ_R) but such that $|\epsilon_I| > \epsilon_R$. These states would be neglected even if they are very narrow. This shortcoming is serious enough to invalidate the criterion above, although it is otherwise appealingly simple.

Another possibility is to include all states in the set of GS irrespective of the value of ϵ_I and to make the selection on the final basis states. For instance, in the particle-hole case studied here, the selection would be done according to the values of the energy difference between the particle and hole states. The disadvantage of this criterion is that it depends on the kind of excitation that one studies (e.g., particle-hole, two-particle–one-hole, etc.). Finally, another criterion is to include in the set of GS only states with values of $|\epsilon_I|$ smaller than a given quantity $\epsilon_I(\text{max})$. We tried different possibilities for $\epsilon_I(\text{max})$. We found the remarkable property that wide GS do not have an appreciable influence upon the giant resonances. This is due to the oscillating characteristics of wide GS. As will be shown below in more detail, absolute values of the radial integrals (21) become smaller the larger the number of contributing oscillations to those integrals is, i.e., the larger $|\epsilon_I|$ is. This property supports our assumption that processes related to observable states may be described by a single-particle representation consisting of GS which are not very wide.

After numerically investigating the different criteria mentioned above, we decided to choose as a set of GS only states with $|\epsilon_I| < 15$ MeV. That is, we consider single-particle resonances wider than 30 MeV to be a part

of the continuum. But it should be noted that this criterion allows for the inclusion of very wide GS, as seen in Table II, and therefore the calculated states may also be very wide.

By using this representation to describe GR's, we hope to retain the advantages of a discrete representation and, in addition, to be able to account for the escape width in a straightforward manner. We avoid the continuous background, as is the case when using harmonic oscillator bases, and we obtain the escape width $\Gamma^\uparrow$ as a by-product of the RPA calculation because $\Gamma^\uparrow$ is simply

TABLE II. The closest single-particle states to the Fermi level in ^{208}Pb calculated by using the computer code GAMOW (Ref. 32) and the potential of Table I. The proton (neutron) energies ϵ_p (ϵ_n) are in MeV. Note that all imaginary values are negative, as it should be for decaying resonant states.

N	State	ϵ_p	ϵ_n
3	$0f_{7/2}$	-22.67	-26.61
3	$0f_{5/2}$	-20.17	-24.78
3	$1p_{3/2}$	-18.32	-23.47
3	$1p_{1/2}$	-17.33	-22.70
4	$0g_{9/2}$	-16.23	-20.99
4	$0g_{7/2}$	-12.37	-18.06
4	$1d_{5/2}$	-11.04	-17.06
5	$0h_{11/2}$	-9.26	-14.96
4	$1d_{3/2}$	-9.10	-15.51
4	$2s_{1/2}$	-8.71	-15.30
5	$0h_{9/2}$	-3.78	-10.69
5	$1f_{7/2}$	-3.54	-10.49
6	$0i_{13/2}$	-1.84	-8.57
5	$2p_{3/2}$	-0.69	-8.35
5	$1f_{5/2}$	-0.52	-8.08
5	$2p_{1/2}$	$0.49 - i0.00$	-7.41
6	$1g_{9/2}$	$4.03 - i0.00$	-3.93
6	$0i_{11/2}$	$5.43 - i0.00$	-2.80
7	$0j_{15/2}$	$5.96 - i0.00$	-1.88
6	$2d_{5/2}$	$6.75 - i0.00$	-2.07
6	$3s_{1/2}$	$7.84 - i0.04$	-1.44
6	$1g_{7/2}$	$8.09 - i0.00$	-0.77
6	$2d_{3/2}$	$8.53 - i0.03$	-0.78
7	$3p_{3/2}$	$12.64 - i1.89$	
7	$2f_{7/2}$	$12.75 - i0.65$	$2.10 - i0.87$
7	$1h_{11/2}$	$11.39 - i0.02$	$2.25 - i0.03$
7	$3p_{1/2}$	$13.22 - i2.50$	
7	$2f_{5/2}$	$14.65 - i1.56$	$2.70 - i2.32$
8	$0k_{17/2}$	$14.06 - i0.00$	$5.03 - i0.00$
7	$1h_{9/2}$	$15.96 - i0.39$	$5.40 - i0.73$
7	$0j_{13/2}$	$15.09 - i0.00$	$5.41 - i0.01$
8	$0i_{13/2}$	$18.14 - i0.57$	$7.66 - i1.04$
8	$3d_{5/2}$	$16.62 - i8.47$	$7.41 - i13.20$
8	$3d_{3/2}$	$17.86 - i10.93$	
8	$4s_{1/2}$	$16.88 - i11.90$	
8	$2g_{9/2}$	$17.84 - i3.55$	$5.54 - i6.38$
8	$2g_{7/2}$	$20.07 - i6.63$	$8.35 - i11.54$
9	$0l_{19/2}$	$22.34 - i0.04$	$12.02 - i0.09$
8	$1i_{11/2}$	$23.24 - i2.52$	$11.33 - i3.94$
8	$2h_{11/2}$	$23.40 - i9.22$	$13.04 - i13.59$
8	$0k_{15/2}$	$24.82 - i0.22$	$13.58 - i0.44$
9	$1j_{15/2}$	$24.68 - i2.31$	$13.22 - i3.52$

TABLE III. The calculated lowest 0^+ states in ^{208}Pb. The uncorrelated energy $E_u = \epsilon_k - \epsilon_i$ is the particle-hole energy corresponding to the given configuration. The correlated states have energies W_n, and their contribution to the isoscalar energy-weighted sum rule is SEWSR. The percentage corresponding to the real part of the SEWSR is also given. Energies are in MeV and the SEWSR is in arbitrary units. The cases where the imaginary energies are not given correspond to bound states.

Configuration	E_u	W_n	SEWSR	%
$\nu(2f_{5/2}1f_{5/2}^{-1})$	$10.64 - i2.32$	$10.68 - i2.31$	$3.0 - i0.2$	4
$\nu(2f_{7/2}1f_{7/2}^{-1})$	$11.81 - i0.87$	$11.78 - i0.80$	$0.1 - i1.0$	0
$\nu(3s_{1/2}2s_{1/2}^{-1})$	13.39	$13.25 - i0.15$	$37.6 - i5.2$	46
$\nu(2d_{3/2}1d_{3/2}^{-1})$	14.09	$13.60 - i0.10$	$23.8 - i3.1$	29
$\nu(2d_{5/2}1d_{5/2}^{-1})$	14.70	$14.10 - i0.03$	$10.3 - i1.3$	13
$\pi(3s_{1/2}2s_{1/2}^{-1})$	$15.85 - i0.04$	$15.10 - i0.05$	$4.6 - i0.9$	6
$\pi(1h_{9/2}0h_{9/2}^{-1})$	$16.17 - i0.73$	$15.94 - i0.04$	$1.0 - i0.3$	1

twice the imaginary part of the resonance energy W_n.

Once the GS have been chosen, we construct the RPA matrix of Eq. (10). We thereby calculate the correlated particle-hole energies W_n and the corresponding forward and backward amplitudes. We will use the separable interaction (15) but including both the isoscalar and isovector components.[27,28] The isoscalar strength κ_0 of the interaction is adjusted, as usual, by fitting the experimental energy of the first excited state. This strength is related to the isovector strength κ_1 and the mixing strength κ' through the relation[28]

$$\kappa_1/\kappa_0 = -\lambda - \tfrac{3}{2}, \quad \kappa'/\kappa_1 = -(N-Z)/A , \qquad (25)$$

where $N-Z$ is the neutron excess and A is the mass number. For the multipole operator we use the form (17) because the corresponding matrix elements are easier to calculate. That is, the integral (21) converges rapidly for this operator. However, we also calculated a large number of cases using (19) and we did not find any appreciable difference, neither in the energies nor in the sum rules, from the cases calculated with (17).

B. Monopole excitations

Giant monopole resonances (GMR's) have been extensively studied during the last decade mainly because of their relation to the incompressibility of nuclear matter.[34] But the important feature for us is that the location and particle decay of the GMR in medium and heavy nuclei has recently been measured. It was found in Ref. 10 that the isoscalar giant monopole resonance (SMR) in ^{208}Pb has a width of 2.4 ± 0.3 MeV and is located at 13.9 ± 0.3 MeV. The decay width was estimated to be about 10% of the total width, that is, about 240 keV. Yet, a more recent measurement[12,13] gives for this width the value

0.425 ± 0.100 MeV. The extraction of these experimental values does not seem to be an easy task. In particular, the particle decay of the SMR may also proceed through preequilibrium. Even the position of the SMR is difficult to determine because it lies in the same energy region as the giant dipole resonance. This was shown in detail in Ref. 35, where the SMR is estimated to lie at 12.9 MeV. Actually, there are a number of different experimental values for this energy. Their average is 13.7 ± 0.3 MeV with a total width of 2.5 ± 0.3 MeV, while it is estimated that the SMR exhausts 94 ± 10% of the isoscalar energy-weighted sum rule (EWSR).[10]

To perform our calculation we used a set of GS which includes states up to the $N=8$ shell with single-particle energies as in Table II except for bound states, where we used experimental energies when available. As in the standard shell-model RPA calculations[36] we found an important redistribution of the uncorrelated EWSR. But in our case both the energies and the EWSR are complex quantities, and the imaginary part of the energy fluctuates considerably from state to state, as seen in Tables III and V. A striking feature of these tables is that the states which exhaust most of the EWSR are narrow, although they may be surrounded by wide states. Moreover, the collective states, i.e., the giant resonances, are not isolated from the neighbor states. This is in contrast with standard calculations, where, for example, the SMR is the first excited state within the corresponding harmonic oscillator shell.[37]

In the case of Table III, the three correlated states at 13.25, 13.60, and 14.10 MeV exhaust 88% of the EWSR, in good agreement with experiment[10] as well as with the results of Ref. 11, where a continuum RPA calculation is performed. Besides, the largest imaginary part of the energies of these collective states is 150 keV, i.e., a width of 300 keV, also in reasonable agreement with the experi-

TABLE IV. Main components of the RRPA wave functions corresponding to the two most collective states in Table III. Only the forward amplitudes are given because the backward amplitudes are negligible.

W_n (MeV)	$\nu(3s_{1/2}2s_{1/2}^{-1})$	$\nu(2d_{3/2}1d_{3/2}^{-1})$	$\nu(2d_{5/2}1d_{5/2}^{-1})$	$\pi(2d_{5/2}1d_{5/2}^{-1})$
$13.25 - i0.15$	$0.78 - i0.15$	$0.34 + i0.10$	$0.26 + i0.10$	$0.25 + i0.08$
$13.60 - i0.10$	$0.69 + i0.17$	$-0.52 + i0.16$	$-0.32 + i0.06$	$-0.22 + i0.06$

TABLE V. Calculated monopole states lying in the energy region of VMR. The isovector energy-weighted sum rule is VEWSR. The rest is as in Table III.

Configuration	E_u	W_n	VEWSR	%
$\pi(1g_{7/2}0g_{7/2}^{-1})$	$19.49-i0.00$	$19.61-i0.00$	$0.4+i0.0$	0
$\pi(1f_{7/2}0f_{7/2}^{-1})$	19.78	$19.95-i0.01$	$1.0+i0.1$	1
$\pi(1g_{9/2}0g_{9/2}^{-1})$	20.26	$20.49-i0.02$	$1.1+i0.1$	1
$\pi(1h_{11/2}0h_{11/2}^{-1})$	$20.74-i0.02$	$22.12-i0.32$	$49.0-i8.2$	60
$\pi(4s_{1/2}2s_{1/2}^{-1})$	$24.89-i11.90$	$24.88-i11.90$	$0.3+i0.3$	0
$\pi(3d_{3/2}1d_{3/2}^{-1})$	$26.21-i10.93$	$26.20-i10.93$	$0.7+i0.6$	1
$\pi(3d_{5/2}1d_{5/2}^{-1})$	$26.29-i8.47$	$26.27-i8.44$	$1.7+i3.1$	2

mental value of about 240 keV mentioned above.

It is interesting to notice that standard shell-model RPA calculations[36] give about the same strength distribution as that shown in Tables III and V. To clarify this we show in Table IV the wave functions of those fragments of the monopole resonance which contribute most to the isoscalar EWSR. Comparing Tables III and IV one clearly sees the reason for that agreement. Namely, our calculated SMR is built up mainly from *bound* GS. This is because the interaction matrix elements corresponding to wide GS are relatively small.

As we mentioned above, the collective state is not the solution with the lowest energy; neither the real part nor the modulus of the energy is the smallest one as should be the case with a harmonic oscillator representation. In Table III the particle-hole configurations lying below the SMR are shown.

In Ref. 29 the imaginary part of the inelastic scattering cross sections was related to the uncertainty of the interference between the resonant process and the corresponding background. For our GR, the imaginary parts of the EWSR are rather small. This means that we could have little doubt about the degree of collectivity given by the real part.

Due to the repulsive character of the isovector interaction,[30] at energies even higher than those analyzed so far lies another collective state, i.e., the isovector giant monopole resonance (VMR) which plays an important role in the total width of the isobaric analog resonances.[38] At such a high energy one would expect that the VMR escape width would be large[39] and the experimental detection of the VMR would be very unlikely. To see how the VMR is built up within our formalism we show in Table V a few states lying in an energy region close to the VMR. It is seen that the giant resonance is narrow, but surrounded by wide states. As before, the collective state is narrow because it is composed of many configurations which are bound or quasi-bound, as seen in Table VI.

The strong collectivity of the VMR as compared to the other 0^+ is manifested in the large number of important components in the corresponding wave function, evenly distributed among neutrons and protons. Most of the correlated states are mainly built on a single particle-hole configuration as, for example, the state lying at $W_n = 24.88 - i11.90$ MeV in Table V which consists virtually of the component $\pi(4s_{1/2}2s_{1/2}^{-1})$.

An important feature to be noted in Table VI is that neutron and proton configurations differ in the sign of the real part of the wave function, as expected for a collective isovector mode. The backward RRPA components both in the isoscalar and in the isovector modes are small, as expected.[40] Yet, these components are needed to obtain a total EWSR which is independent of the residual interaction.[41] We use this feature to check our calculations.

In our calculation the VMR exhausts only 60% of the EWRS and the rest is spread over small pieces in other regions, as shown in Table VII.

Probably the most important result of our calculation is the small escape width obtained for the giant monopole resonances. This is only a manifestation of the fact that both the isoscalar and the isovector resonances are built upon bound or quasi-bound configurations. While this feature explains why our giant resonances are located at about the same energies than those calculated with harmonic oscillator bases, the small escape width of our VMR is an unexpected result.[42]

C. Quadrupole excitations

The experimental data on isoscalar quadrupole giant resonances in ^{208}Pb are rather abundant,[35,43,44] and their analysis within the RRPA was therefore useful to check the reliability of the method[14] as well as to get new insight into the structure of the giant resonances.

Here we present the results of the calculation corresponding to the isovector quadrupole giant resonance (VQR).

Using the same set of GS as in the monopole case analyzed in the preceding section, we obtained the states shown in Table VIII. The VQR has an escape width of 1 MeV. This is wider than the VMR but still rather nar-

TABLE VI. The six largest components of the VMR wave function. $\nu(\pi)$ labels neutron (proton) configurations.

ν	$(0.31+i0.02)(1g_{9/2}0g_{9/2}^{-1})$ $(0.29+i0.01)(1h_{11/2}0h_{11/2}^{-1})$ $(0.24+i0.02)(1g_{7/2}0g_{7/2}^{-1})$	
π	$-(0.59+i0.03)(1h_{11/2}0h_{11/2}^{-1})$ $-(0.40+i0.01)(1g_{9/2}0g_{9/2}^{-1})$ $-(0.25+i0.00)(1f_{7/2}0f_{7/2}^{-1})$	

TABLE VII. The nine states which exhaust most of the monopole VEWSR. Units and notation as in Table III.

W_n	VEWSR	%
18.06 − i0.02	1.06 − i.02	2
19.95 − i0.01	1.0 + i0.1	1
20.49 − i0.02	1.1 + i0.1	1
22.12 − i0.32	49.0 − i8.2	60
26.27 − i8.44	1.7 + i3.1	2
28.11 − i13.48	5.3 − i1.3	6
31.48 − i6.62	1.7 + i1.5	2
32.82 − i9.22	9.1 − i2.1	11
45.11 − i8.47	1.5 + i0.3	3

row in comparison to the other states contributing to the isovector EWSR. From Table VIII one sees that the VQR is surrounded by very wide and noncollective states. We tried to understand why the VQR is so narrow by analyzing the VQR wave function. We found that it mainly consists of configurations with high spin single-particle states, as seen in Table IX. These states are either bound or quasi-bound and, as already mentioned, the wider the corresponding GS, the smaller the matrix elements (21). At the same time, the particle and the hole in the neutron configurations of Table IX are aligned, giving a large contribution to the quadrupole transition matrix elements. The proton configurations correspond also to narrow GS, but the alignment is not so remarkable. These configurations are important because the proton states in Table IX lie very close to the VQR.

It is actually this combination of quasi-bound states with enhanced transition matrix elements which explains the success of real representations in describing the strength distribution of the quadrupole giant resonances. The structure of the wave function in Table IX also explains why the calculated escape width of the VQR is rather small.

A remarkable feature in Table VIII is that the EWSR of the VQR has a large imaginary part. This suggests that there is a strong interference with the background, impairing a probable experimental detection of the VQR.

Finally, we increased the size of the GS basis by 20%, but neither the energies nor the EWSR of the states discussed here changed significantly, showing that these correlated states are indeed contained in the subspace

TABLE VIII. Quadrupole states around the VQR. Units and notation as in Table III.

W_n	VEWSR	%
22.92 − i13.20	0	0
22.92 − i15.29	0	0
23.14 − i15.29	0	0
23.31 − i0.51	340 − i230	70
23.57 − i13.53	8 + i4	2
23.60 − i6.37	i2	0
23.73 − i13.59	0	0

spanned by the GS chosen according to the criterion discussed in Sec. IV A.

D. Octupole and hexadecapole excitations

Since the strength corresponding to a given multipolarity is spread over a larger energy range for larger angular momenta, excitations of multipolarity higher than quadrupole are difficult to analyze experimentally. Moreover, the isoscalar pieces of many giant resonances lie just at about the same energy,[42] blurring the identification of any of them. In spite of all these difficulties, a number of experiments have recently been performed detecting resonances of high multipolarity.[35,42]

The octupole resonances best studied in the lead region are the low-energy isoscalar ones which are mainly built upon $\Delta N = 1$ excitations.[45] Also at higher energies, important broad pieces of the same isoscalar resonances, but built upon higher ΔN excitations, were recently measured.[42] To study these resonances we included in our representation excitations up to $\Delta N = 5$.

The states obtained by diagonalizing the RRPA matrix have to a large extent the same features as the quadrupole states. That is, giant resonances are built upon high-spin GS and they are always narrow.

One notices in the calculated spectrum that there is a rather large fragmentation of the isoscalar octupole strength. The low-energy region, i.e., up to 7 MeV, contains essentially one large piece at 2.62 MeV, which is the low-lying octupole vibration, exhausting 22% of the EWSR. This is in good agreement with the experimental value[45] of 20.4%. At 6 MeV we have another concentration of strength exhausting 4% of the EWSR, which does not fit the experimental value of 15.2% at 5.4 MeV well. However, neither the good agreement of the lowest octupole vibration nor the poor one of the others is an exclusive feature of the RRPA. Both features are common to a number of other calculations.[45]

At about 19 MeV we have also obtained a large portion of the isoscalar octupole strength. This is the high-energy octupole resonance (HEOR). In our calculation the HEOR exhausts 28% of the EWSR while experimentally there are very large differences,[42] from 20±6% up to 220^{+80}_{-100}%. But the position of the HEOR is given well by the RRPA, although this is also a feature present in shell-model RPA calculations.[37]

Our calculated isovector giant resonance lies at about 31 MeV and has an escape width of about 1.5 MeV, which is rather narrow considering its high excitation energy. The isovector strength is strongly concentrated in the giant resonance, and its imaginary part is less than 10% of the real part, as seen in Table X. This is a nice feature which would make this resonance an outstanding candidate to be searched experimentally, although it seems to be difficult to generate a probe which would specifically excite the isovector mode.[44]

All the other important pieces of the octupole giant resonances are also narrow, and the imaginary parts of their strengths are small. For instance, the isoscalar excitation at 18.73 MeV has an EWSR of 327 + i6 (in arbi-

TABLE IX. Main components of the VQR. Note the difference in sign between neutron and proton amplitudes.

W_n (MeV)	$\nu(0k_{17/2}0i^{-1}_{13/2})$	$\nu(0j_{13/2}0h^{-1}_{9/2})$	$\pi(2d_{5/2}0g^{-1}_{9/2})$	$\pi(1g_{7/2}0g^{-1}_{9/2})$
$23.34-i0.51$	$0.26+i0.02$	$0.22+i0.01$	$-0.50-i0.07$	$-0.35+i0.07$

trary units). This exhausts 30% of the total EWSR.

The small widths of the octupole GR's are a consequence of the structure of their wave functions, which, as usual, mainly consist of high spin GS. As an example, we show in Table XI the wave functions of the isoscalar and isovector HEOR. The strong collectivity of the isovector mode is seen in that the wave function is spread in many equally important configurations. Moreover, all components of the wave functions in Table XI have the spins of the particle and the hole aligned. Also, in all cases the orbital angular momentum of the particle is the maximum possible. This facilitates the "trapping" of the particle within the nucleus, hindering the decay of the giant resonance. This feature is even more pronounced here than in the quadrupole case discussed above.

Finally we calculated the hexadecapole states. The isoscalar strength of the hexadecapole mode is rather frag-

mented, but three distinct regions of the spectrum can be observed. At 4.32 MeV lies the low-energy hexadecapole vibration which exhausts 7% of the isoscalar EWSR. At about 12 MeV, just in the same region where the monopole and the quadrupole isoscalar resonances lie, a concentration of strength exhausting 22% of the EWSR is found. This agrees rather well with the experimental value of 10 ± 3 % of Ref. 46 and with the value of $\approx30\%$ of Ref. 47. Besides, in the SQR region a strength of 23–29 % was estimated for the hexadecapole mode in Ref. 48. But our calculated value differs from the experimental one of 62 ± 20 % given in Ref. 42.

At about 27 MeV a strong isoscalar resonance appears which mainly corresponds to $\Delta N=4$ excitations, as is seen from the corresponding wave function. The imaginary part of this wave function is negligible, while the four most important real components are

$$|4^+;E=26.97-i0.06\text{ MeV}\rangle=|0.84\nu(0l_{19/2}0h^{-1}_{11/2})+0.33\pi(0j_{15/2}0f^{-1}_{7/2})+0.22\pi(0k_{17/2}0g^{-1}_{9/2})$$
$$+0.19\pi(0l_{19/2}0h^{-1}_{11/2})\rangle\ .$$

Again in this case one sees, through the sign and the alignment features of the wave function components, the reason for the collectivity of this state as well as for its small escape width. This resonance exhausts 23% of the EWSR and it may correspond to the high-energy resonance, exhausting 20 ± 10 % of the EWSR reported in Ref. 42.

In the isovector spectrum one does not see the strong concentration of strength found in the corresponding octupole mode. This, and the fact that the isovector hexadecapole resonance lies at very high energy, indicates that its experimental detection is improbable.

V. SUMMARY AND CONCLUSIONS

In this paper we have presented a formalism to describe nuclear properties of states lying in the continuum.

TABLE X. The five states which exhaust most of the octupole isovector VEWSR. Units and notation as in Table III.

W_n	VEWSR	%
$26.29-i0.07$	$20+i16$	2
$27.01-i0.09$	$28-i3$	2
$30.65-i0.77$	$1065-i102$	89
$32.29-i6.29$	$31+i43$	3
$34.13-i0.24$	$21-i18$	2

The representation used in this formalism, which we call GS, consists of both bound single-particle states and resonances with outgoing boundary conditions (Gamow resonances) being solutions of the Schrödinger equation with a Woods-Saxon potential. The states (GS) cannot be normalized in the usual meaning of this term, but we have shown how this problem can be overcome. Thereby we used for the GS the completeness relation of Berggren.[15] Although Gamow resonances are perpendicular to any real state, they have the peculiar property of having a large overlap with wave packets centered in the resonances.[23] Making use of this property and guided by the shell-model prescription to select a physically meaningful representation, we have established a criterion to choose a set of GS adequate to describe *observable* quantities. This allows one to calculate rather straightforwardly the decay properties of correlated states. In this paper we have given the RPA equations for particle-hole excitations (RRPA). The imaginary part of the calculated energies is half of the escape width of the corresponding states. We have also presented the expression corresponding to the energy-weighted sum rule (EWSR) for the decay of the RRPA states. The fragmentation of the EWSR was identified with the Landau damping of the GR concerned. Using a separable interaction we obtained a complex dispersion relation which we discussed in detail and showed how to solve it by a graphical method. The graphical method opened some insight on

TABLE XI. Main components of the wave functions corresponding to the isoscalar octupole resonance at 18.73 MeV and the corresponding isovector resonance at 30.65 MeV.

W_n	$\nu(0j_{15/2}0g_{9/2}^{-1})$	$\nu(0k_{17/2}0h_{11/2}^{-1})$	$\pi(0i_{13/2}0f_{7/2}^{-1})$	$\pi(0k_{17/2}0h_{11/2}^{-1})$
$18.73+i0.00$	$0.61-i0.01$	$0.22+i0.00$	$0.35+i0.00$	$0.28+i0.00$
$30.65-i0.77$	$0.20+i0.01$	$0.26+i0.02$	$-0.13-i0.00$	$-0.30-i0.00$

how the collective states are built from several p-h components as the strength of the interaction increases.

We applied the RRPA formalism to study giant resonances in ^{208}Pb. Since the particle decay properties of these resonances have recently been the subject of several experiments[10-13] the calculation of the corresponding widths is of actual interest. We found that in all cases the escape widths of giant resonances are not large. This is partially due to the fact that transition matrix elements are smaller the wider are the states connected by the transition operator. But it is also a manifestation of the structure of the resonances, especially those with high multipolarities. The main configurations of the giant resonance wave functions have the spins of the particle and the hole aligned with the angular momentum of the transition operator. This enhances the transition probabilities because the angular momentum recoupling coefficients acquire in this case their maximum values. Moreover, to also obtain the maximum overlap between the initial and final radial wave functions in the transition matrix elements it is necessary that the difference in the number of nodes of those functions is as small as possible. This is indeed the case, because for a given value of ΔN a minimum value of Δn implies a maximum for Δl.

Since the hole in the particle-hole giant resonance is in a bound (i.e., low-spin) state, the alignment mentioned above requires that the particle move in a high angular momentum orbit. Therefore, the corresponding centrifugal barrier tends to trap this particle within the nuclear volume, hindering the particle decay of the giant resonance. This also explains the success of harmonic oscillator representations in describing giant resonances.

The calculated escape widths agree reasonably well with available experimental data. Among the states which have not been observed so far, our calculation predicts that a candidate likely to be observed is the octupole isovector giant resonance, with 89% of its strength concentrated at about 31 MeV and an escape width of about 1.5 MeV.

*On leave from Institute of Nuclear Research of the Hungarian Academy of Sciences, H-4001 Debrecen, Pf. 51, Hungary.

[1]C. Mahaux and H. A. Weidenmüller, *Shell Model Approach to Nuclear Reactions* (North-Holland, Amsterdam, 1969).

[2]S. Shlomo and G. Bertsch, Nucl. Phys. **A243**, 507 (1975).

[3]G. Co and S. Krewald, Nucl. Phys. **A433**, 392 (1985).

[4]R. DeHaro, S. Krewald, and J. Speth, Nucl. Phys. **A388**, 265 (1982).

[5]B. Buck and A. D. Hill, Nucl. Phys. **A95**, 271 (1967).

[6]S. Stringari and D. Vautherin, Phys. Lett. **88B**, 1 (1979).

[7]Ph. Chomaz, Nguyen Van Giai, and S. Stringari, Phys. Lett. B **189**, 375 (1987).

[8]Nguyen Van Giai, P. F. Bortignon, F. Zardi, and R. Broglia, Phys. Lett. B **199**, 155 (1987).

[9]H. Ejiri, J. Phys. (Paris) **45**, C4-135 (1984).

[10]S. Brandenburg, W. T. A. Borghols, A. G. Drentje, L. P. Ekström, M. N. Harakeh, A. van der Woude, A. Hakanson, L. Nilsson, N. Olsson, M. Pignanelli, and R. De Leo, Nucl. Phys. **A466**, 29 (1987).

[11]K. Fuchs, W. Eyrich, A. Hofmann, B. Mühldorfer, U. Scheib, H. Schlösser, and H. Rebel, Phys. Rev. C **32**, 418 (1985).

[12]A. Bracco, J. R. Beene, F. E. Bertrand, M. L. Halbert, D. C. Hensley, R. L. Auble, D. J. Horen, R. L. Robinson, and R. O. Sayer, Oak Ridge National Laboratory, Physics Division Progress Report, 1987.

[13]A. Bracco, J. R. Beene, N. Van Giai, P. F. Bortignon, F. Zar-

di, and R. A. Broglia, Phys. Rev. Lett. **60**, 2603 (1988).

[14]T. Vertse, P. Curutchet, O. Civitarese, L. S. Ferreira, and R. J. Liotta, Phys. Rev. C **37**, 876 (1988).

[15]T. Berggren, Nucl. Phys. **A109**, 265 (1968).

[16]G. Gamow, Z. Phys. **51**, 204 (1928).

[17]W. J. Romo, Nucl. Phys. **A419**, 333 (1984).

[18]A. F. J. Siegert, Phys. Rev. **56**, 750 (1939).

[19]Y. B. Zel'dovich, Zh. Eksp. Teor. Fiz. **39**, 776 (1960) [Sov. Phys.–JETP **12**, 542 (1961)].

[20]W. J. Romo, Nucl. Phys. **A116**, 617 (1968).

[21]B. Gyarmati and T. Vertse, Nucl. Phys. **A160**, 573 (1971).

[22]B. Simon, Phys. Lett. **73A**, 211 (1979).

[23]J. Aguilar and J. M. Combes, Commun. Math. Phys. **22**, 269 (1971); E. Balslev and J. M. Combes, *ibid.* **22**, 280 (1971).

[24]P. Ring and P. Schuck, *The Nuclear Many Body Problem* (Springer Verlag, New York, 1980).

[25]T. Vertse, P. Curutchet, and R. J. Liotta, in *Proceedings of the Symposium on Resonances—the Unifying Route Towards the Formulation of Dynamical Processes, Wärmland, Sweden, 1987*, edited by N. Elander and E. Brandas (Springer Verlag, New York, in press).

[26]A. M. Lane, *Nuclear Theory* (Benjamin, Reading, Mass., 1964).

[27]D. R. Bes, R. A. Broglia, and B. S. Nilsson, Phys. Rep. **16C**, 1 (1975).

[28]A. Bohr and B. Mottelson, *Nuclear Structure* (Benjamin, New

York, 1975), Vol. 2.

[29] T. Berggren, Phys. Lett. **73B**, 389 (1978).

[30] G. F. Bertsch, *The Practitioner's Shell Model* (North-Holland, Amsterdam, 1972).

[31] Numerical Algorithms Group, Library Manual, Oxford, 1982.

[32] T. Vertse, K. F. Pál, and Z. Balogh, Comput. Phys. Commun. **27**, 309 (1982).

[33] L. Rydström and J. Blomqvist, Research Institute of Physics, Stockholm, Annual Report, 1980, p. 86.

[34] J. P. Blaizot, Phys. Rep. **64C**, 171 (1980).

[35] F. E. Bertrand, E. E. Gross, D. J. Horen, R. O. Sayer, T. P. Sjoreen, D. K. McDaniels, J. Lisantti, J. R. Tinsley, L. W. Swenson, J. B. McClelland, T. A. Carey, K. Jones, and S. J. Seestrom, Phys. Rev. C **34**, 45 (1986).

[36] K. Goeke and J. Speth, Annu. Rev. Nucl. Sci. **32**, 65 (1982).

[37] J. Wambach, F. Osterfeld, J. Speth, and V. A. Madsen, Nucl. Phys. **A324**, 77 (1979).

[38] N. Auerbach, Nucl. Phys. **A182**, 247 (1972).

[39] W. M. MacDonald and M. C. Birse, Phys. Rev. C **29**, 425 (1984).

[40] J. Wambach, V. K. Mishra, and Li Chu-Hsia, Nucl. Phys.

[A380], 285 (1982).

[41] D. J. Thouless, Nucl. Phys. **22**, 78 (1961).

[42] B. Bonin, N. Alamanos, B. Berthier, G. Bruge, H. Faraggi, D. Legrand, J. C. Lugol, W. Mittig, L. Papineau, A. I. Yavin, D. K. Scott, M. Levine, J. Arvieux, L. Farvacque, and M. Buenerd, Nucl. Phys. **A430**, 349 (1984).

[43] G. F. Bertsch, P. F. Bortignon, and R. A. Broglia, Rev. Mod. Phys. **55**, 287 (1983).

[44] F. E. Bertrand, Nucl. Phys. **A354**, 129c (1981).

[45] Y. Fujita, M. Fujiwara, S. Morinobu, I. Katayama, T. Yamazaki, T. Itahashi, H. Ikegami, and S. I. Hayakawa, Phys. Rev. C **32**, 425 (1985), and references therein.

[46] J. R. Tinsley, D. K. McDaniels, J. Lisantti, L. W. Swenson, R. Liljestrand, D. M. Drake, F. E. Bertrand, E. E. Gross, D. J. Horen, and T. P. Sjoreen, Phys. Rev. C **28**, 1417 (1983).

[47] H. P. Morsch, P. Decowski, M. Rogge, P. Turek, L. Zemlo, S. A. Martin, G. P. A. Berg, W. Hürlimann, J. Meissburger, and J. G. M. Römer, Phys. Rev. C **28**, 1947 (1983).

[48] T. Yamagata, S. Kishimoto, K. Iwamoto, K. Yuasa, M. Tanaka, S. Nakayama, T. Fukuda, M. Inoue, M. Fujiwara, Y. Fujita, I. Miura, and H. Ogata, Phys. Lett. **123B**, 169 (1983).